Published in final edited form as:

Angew Chem Int Ed Engl. 2023 September 11; 62(37): e202308086. doi:10.1002/anie.202308086.

A Semisynthetic Bioluminescence Sensor for Ratiometric Imaging of Metal Ions *In Vivo* Using DNAzymes Conjugated to An Engineered Nano-Luciferase

Mengyi Xiong[‡,a], **Yuting Wu**[‡,b], **Gezhi Kong**[a], **Whitney Lewis**[b], **Zhenglin Yang**[b], **Hanxiao Zhang**[c], **Li Xu**[a], **Ying Liu**[a], **Qin Liu**[a], **Xuhua Zhao**[c], **Xiao-Bing Zhang**[a], **Yi Lu**[b]

[a]Molecular Science and Biomedicine Laboratory, State Key Laboratory of Chemo/Biosensing and Chemometrics, College of Chemistry and Chemical Engineering, Hunan University, Changsha, Hunan 410082 (PR China)

[b]Department of Chemistry, University of Texas at Austin, Austin, Texas 78712 (United States)

[c]Department of Biochemistry and Molecular Biology, Shanxi Medical University, Taiyuan, Shanxi 030001 (RP China)

Abstract

DNA-based probes have gained significant attention as versatile tools for biochemical analysis, benefiting from their programmability and biocompatibility. However, most existing DNA-based probes rely on fluorescence as the signal output, which can be problematic due to issues like autofluorescence and scattering when applied in complex biological materials such as living cells or tissues. Herein, we report the development of bioluminescent nucleic acid (bioLUNA) sensors that offer laser excitation-independent and radiometric imaging of the target *in vivo*. The system is based on computational modelling and mutagenesis investigations of a genetic fusion between circular permutated Nano-luciferase (NLuc) and HaloTag, enabling the conjugation of the protein with a DNAzyme. In the presence of Zn^{2+}, the DNAzyme sensor releases the fluorophore-labelled strand, leading to a reduction in bioluminescent resonance energy transfer (BRET) between the luciferase and fluorophore. Consequently, this process induces ratiometric changes in the bioluminescent signal. We demonstrated that this bioLUNA sensor enabled imaging of both exogenous Zn^{2+} *in vivo* and endogenous Zn^{2+} efflux in normal epithelial prostate and prostate tumors. This work expands the DNAzyme sensors to using bioluminescence and thus has enriched the toolbox of nucleic acid sensors for a broad range of biomedical applications.

Graphical Abstract:

A fusion protein of Nano-luciferase and HaloTag was engineered to construct a DNAzyme sensor for metal ion detection *in vivo*, utilizing bioluminescent resonance energy transfer (BRET).

xbzhang@hnu.edu.cn, yi.lu@utexas.edu.

‡These authors contributed equally to this work.

Twitter handle: @LuLabUT

Supporting information for this article is given via a link at the end of the document.

Keywords

Nucleic acid sensor; DNAzyme; Bioluminescence; Protein engineering; *In vivo* imaging

Introduction

Metal ions play vital roles in numerous essential activities within living systems, encompassing functions such as osmotic regulation, catalysis, metabolism, biomineralization, and signaling.[1] Both deficiencies and excess of metal ions have been implicated in the development of various diseases, including anemia, neurodegenerative disorders, and cancers.[2] Consequently, the detection and quantification of different metal ions in cells or tissues are crucial not only for unraveling their regulatory mechanisms in physiological environments but also for gaining valuable insights into potential therapeutic approaches. To achieve these objectives, instrumental techniques such as atomic absorption spectroscopy (AAS),[3] inductively coupled plasma mass spectrometry (ICP-MS)[4] and X-ray fluorescence microtomography[5] are employed for the measurement of metal ions. These techniques are sophisticated in measuring metal ions in bulk samples, detecting the speciation, distribution, and accessibility of metals in cells, tissues, and whole organisms in living bodies is still a challenge. To overcome these limitations, probes based on a variety of molecules, including small molecules,[6] polymers,[7] and proteins[8] have been reported. While these probes have successes in detecting some metal ions, it has been difficult to apply the methods generally to detecting other metal ions because it is quite challenging to rationally design these sensors with high selectivity against other metal ions and species. In addition, most of these sensors requires careful design and synthesis of molecules that can not only bind metal ions selectively, but also couple the binding into detectable signals such as fluorescence. As a result, there are only a limited number of metal ion probes.

To overcome these limitations and broaden the scope of metal ion detection, DNAzymes, a class of DNA molecules that perform an enzymatic function by using target metal ions as cofactors, have emerged as a promising alternative. Through the process of *in vitro* selection, DNAzymes with high selectivity for a wide range of metal ions can be obtained.[9] The metal ion-selective binding and DNAzyme activity can be readily transformed into fluorescent signals by conjugating a fluorophore/quencher pair to the ends of two hybridizing DNA strands and utilize the difference of melting temperatures before and after metal ion-dependent cleavage. This approach has been successfully employed to develop DNAzyme-based fluorescent probes for numerous metal ions, including Li^+, Na^+, Ag^+, Mg^{2+}, Zn^{2+}, Ca^{2+}, Cu^+/Cu^{2+}, Fe^{2+}/Fe^{3+}, Mn^{2+}, Pb^{2+}, $UO_2{}^{2+}$, Hg^{2+}, and Cd^{2+}.[10] Since this approach separates the DNA domain for selective binding to metal ions from the fluorophore/quencher for signaling output, the DNAzyme sensors can readily utilize different fluorophores for signaling without compromising selectivity. Despite the progress, only a few of these DNAzyme probes have been applied for *in vivo* imaging in animals and other species.[11] The limited application of fluorescent sensors for *in vivo* imaging is partially attributed to challenges associated with autofluorescence and scattering from tissues, which arise from the use of exciting lasers to activate the fluorescent probes.[12] This

autofluorescence and scattering contributes to a poor signal-to-noise ratio and decreased sensitivity, which largely hampers their applicability for *in vivo* imaging.

Bioluminescent techniques provide a promising solution for low background bioimaging. Bioluminescence is a chemical process that relies upon the interaction of an enzyme, termed luciferase, and substrate that produce "cold light".[13] Bioluminescence offers an advantage over fluorescence that it does not require external excitation. As a result, bioluminescence can minimize the background signal caused by autofluorescence and scattering, which are often generated by the external excitation of complex biological materials such as living cells or tissues. Importantly, bioluminescence can also avoid photobleaching and the generation of toxic radicals, thus allowing for prolonged measurements.[14] Given such features, bioluminescence is extensively used in the investigation of protein-protein interactions, exploring gene regulation and cell signaling, as well as being converted into biosensors for point-of-care (POC) assays in complex samples and for *in vivo* bioluminescence imaging.[15] Despite their potential, most of these sensors are genetically encoded sensors or semisynthetic sensors that require protein tagging and analyte analog modules. In contrast, bioluminescent sensors based on DNA have rarely been explored, due to the difficulty in building the connection between luciferase and DNA sensors.[16] Although commercialized Renilla Luciferase-Streptavidin fusion protein could modify the luciferase onto biotinylated DNA, the energy transfer efficiency is usually insufficient for *in vivo* applications because of the long distance between luciferase and DNA molecules due to the size of streptavidin-biotin complex and the limitations caused by the Renilla luciferase on its size, stability, and luminescence efficiency.[15a]

To meet such a challenge, we report herein a versatile and generalizable method to construct bioluminescent nucleic acid (bioLUNA) sensors for ratiometric detection of metal ions *in vitro* and *in vivo*. As shown in Scheme 1, the sensor consists of two moieties. The first is the signaling readout moiety consisting of a fusion protein with an engineered circular permutated Nano-luciferase (cpNLuc), which is 150-fold brighter than traditional luciferase, and a HaloTag, whose labeling site is close to the catalytic domain of cpNLuc. This moiety allows both the biorthogonal labeling of DNA sensors and the generation of bioluminescence signals. The second moiety is a Zn^{2+}-specific DNAzyme, which serves as the metal ions sensing part that ensures the sensor response to the metal ion. The 3' terminal of the DNAzyme strand is conjugated with a chloroalkane for the connection to the fusion protein and the 5' end of the substrate strand is modified with a fluorophore. After hybridizing the enzyme strand and the substrate strand, the fluorophore is close to the catalytic site of cpNLuc and an effective BRET occurs between cpNLuc and the fluorophore upon addition of the furimazine substrate. Once the DNAzyme is activated by Zn^{2+}, the substrate strand will be cleaved into two shorter product strands. Due to the length change of the cleaved product, the melting temperature of the fluorophore-labeled cleavage product strands and the enzyme strand is reduced and becomes lower than room temperature. Thus, the product strand dehybridizes from the enzyme strand, which releases the fluorescent moiety spatially away from the cpNLuc, resulting in a dramatic change of the BRET signal. Given the advantages of the high signal-to-background ratio and brightness, the sensor realized sensing both exogenous Zn^{2+} *in vivo*, as well as endogenous Zn^{2+} efflux

in normal epithelial prostate and prostate tumors. This sensor provides a powerful tool for the comparison of Zn^{2+} concentrations between animals with and without prostate tumor.

Results and Discussion

Rational design and engineering of the luciferase-HaloTag fusion protein for labelling oligonucleotides

To design a BRET bioLUNA sensor with the superior performance of signal transformation, several key factors should be fulfilled: (1) high brightness of the bioluminescence when the luciferase reacts with its substrate; (2) short distance between the bioluminescence generating site on luciferase and the signal acceptor on DNA sensor; (3) high efficiency of labeling the DNA sensor with luciferase. To meet these challenges, we chose a previously reported circular permutated HaloTag-NLuc fusion protein, which consists of an engineered Nano luciferase with superior brightness in the reaction with furimazine and a HaloTag protein for bioorthogonal labeling.[17] To facilitate the proximity of the catalytic site responsible for processing the furimazine substrate on cpNLuc and the self-labeling site on HaloTag, the HaloTag protein is split between 155Thr and 157Asp and fused with cpNLuc. This strategic fusion allows for the efficient interaction between the two domains, enabling the catalytic function of cpNLuc and the self-labeling ability of HaloTag without compromising the brightness of the luciferase or the self-labeling capacity of the HaloTag with chloroalkane-contained groups.[18] Despite these features, our molecular structure modeling of this cpHNLuc protein indicates that its labeling pocket of the split HaloTag is exposed closely to the NLuc (Figure 1A), resulting in a substantial steric hindrance to capture the chloroalkane-modified DNA. As demonstrated in Figure S1, the labeling efficiency of $cpHNLuc_0$ to the DNA was only 20.4%, while the C terminal fusion of HaloTag to NLuc achieved a labeling efficiency of 63.8%. Additionally, the surface electrostatic potentials of the fusion protein further revealed that the labeling site of HaloTag was surrounded by negatively charged amino acid residues (AARs), which may reduce the labeling efficiency due to the electrostatic interactions between the negatively charged oligonucleotides and protein. This modeling prediction was validated by experimental results, which showed a low labeling efficiency of 20% in the cpHNLuc reaction with oligonucleotides (see Figure 2B and Figure S3 for $cpHNLuc_0$). Therefore, the existing cpHNLuc is unsuitable for the construction of nucleic acid sensors based on BRET.

Based on the above observations and inspired by previous research demonstrating enhanced reaction efficiency of HaloTag protein by adjusting its surface potential,[19] we hypothesize that replacing the negatively charged AARs close to the DNA labeling site with positively charged AARs would potentially enhance the efficiency of the DNA labeling reaction, by reducing the intermolecular electrostatic repulsion between the split HaloTag and negatively charged oligonucleotides. However, if too many positively charged AARs are introduced to the HaloTag, they might hinder the labeling reaction by causing intramolecular competition between the positively charged AARs and the DNA labeling site in attracting the negatively charged oligonucleotides. Therefore, it was crucial to evaluate the target mutation sites to find a right balance between the two competing forces. A previous study suggested that the amino acid residues from P152 to Q175 in the alpha-helical structures of HaloTag

(PDB: 4KAF) were potential sites for mutation.[19a] Even if the alpha helix was cleaved into two fragments (P143-155T and D339-Q348) in cpHNLuc, they were still shown to be amenable to mutations with minimal structural perturbation. The molecular modeling demonstrated that the mutations of the negatively charged Glu144, Glu148, and Asp339 to positive charged lysine (K) would effectively reverse the local electrostatic potential around the labeling site of the cpHNLuc (Figure 1B). Additionally, the negative charged Glu353, Glu366, and Glu368 in V350-G359 and E366-R373 alpha helixes were also chosen as potential mutation sites against intermolecular electrostatic repulsion, and they were changed to lysine stepwise (Figure 1C).

As a result of the above molecular modeling, we have rationally designed a series of variants of cpHNLuc containing single, double, or multiple mutations (Figure 1D). They were constructed and expressed in *Escherichia coli* followed by purification using Ni-chelating affinity chromatography. When assessed by SDS-PAGE, all the variants were well expressed except cpHNLuc$_7$, which brings unwanted side products due to low expression yield (Figure S2). Thus, the cpHNLuc$_0$ to cpHNLuc$_6$ variants (see protein sequence in Table S4) were adopted for the following investigations.

The capability of the cpHNLuc variants for engineering the bioLUNA sensors

To investigate the ability of these proteins to bind oligonucleotides, a chloroalkane-modified ssDNA L21 (see the sequence in Table S3) was incubated with the variants because the chloroalkane has been shown to be covalently conjugated to the Asp106 amino acid via a self-catalytic reaction (Figure 2A).[20] The time-dependent reactions of these variants with the oligonucleotide were monitored via SDS-PAGE (Figure S3), which were further quantified by the kinetic curves (Figure 2B) and the parameters can be found in Table S1. We demonstrated that the single mutation at E144K or E148K (cpHNLuc$_1$ and cpHNLuc$_2$) would increase the labeling efficiency from 20.6% of the wide type cpHNLuc$_0$ to 37.2% and 33.5%, respectively, confirming our predication from the modeling study that the positively charged AARs around this labeling site could accelerate the labeling reaction. Since both E144K and E148K single mutation was effective in increasing the labeling efficiency, we combined the two mutants in cpHNLuc$_3$, resulting in a remarkable improvement of labeling efficiency to 79.7% and a rate constant of 0.18 min^{-1} which was 15-fold higher than the wide type cpHNLuc$_0$. Interestingly, further addition of the D339K mutation (cpHNLuc$_4$) resulted in an even higher labeling efficiency of 91.6% and a rate constant of 0.31 min^{-1}. This labeling efficiency was demonstrated to be independent from the length or sequence of DNA strands (Figure S4).

To further maximize labeling efficiency, we replaced the Glu353 and Glu366 in V350-G359 and E366-R373 alpha helices near the labeling site with lysine to generate cpHNLuc$_5$ and cpHNLuc$_6$ (Figure 1C). The cpHNLuc$_5$ and cpHNLuc$_6$ displayed slightly increased labeling efficiency of 93.8% and 92.0% in comparison with cpHNLuc$_4$ (Table S1), demonstrating the E353K and E366K could reduce the intermolecular electrostatic repulsion which benefits the final efficiency of oligonucleotides labeling. However, the rate constants of the reaction dropped significantly to 0.11 min^{-1} and 0.09 min^{-1}, probably because the over-mutation resulted in an unwanted intramolecular competition that hamper the labeling

rate. Collectively, our findings suggest that cpHNLuc$_4$ represents a promising candidate variant capable of striking a delicate balance between intermolecular electrostatic repulsion and intramolecular competition.

In addition to the labeling efficiency, the properties of bioluminescence, including brightness and energy transferring efficiency, are the important questions that we evaluated next for these variants. Since the mutations were entirely conducted on the HaloTag region of the fusion protein, the ability to generate bioluminescence by these luciferase proteins should not be affected. We found that all the variants exhibited comparable brightness to the original cpHNLuc$_0$ in the reaction with furimazine, and the cpHNLuc$_4$ showed even approximately 190% higher brightness after the labeling of oligonucleotide (Table S1). The capability of the variants in the signal transformation was also evaluated by testing the BRET ratio between the protein and sensors, by incubating the proteins with a chloroalkane and Cy3 dual-labeled DNA molecular beacon (cpHNLuc-MB), so that the Cy3 receptor was near the catalytic site of cpNLuc. The bioluminescent spectrums of this cpHNLuc-MB were then collected with the supply of furimazine. As displayed in Figure 2C, the cpHNLuc$_3$, cpHNLuc$_4$, cpHNLuc$_5$ and cpHNLuc$_6$ showed high BRET ratios (565 nm / 450 nm), among which the cpHNLuc$_4$ possessed the best BRET with a ratio of 3-fold. The emission color of those sensors also turned from blue to red with the increased BRET ratio (565 nm / 450 nm). After treatment with DNase I, an endonuclease that degrades oligonucleotide, the BRET ratio decreased, while the color of emission light returned to blue (Figure S5). Moreover, no BRET was observed when the protein was incubated with a non-chloroalkane-labeled DNA hairpin (Figure S6). These observations indicate that the BRET signals were caused by the conjugation of the DNA to proteins. Also, cpHNLuc$_4$ was a promising candidate for the construction of bioLUNA sensors due to its high labeling efficiency, brightness of bioluminescence intensity, and high energy transfer when conjugated with a DNA sensor. To investigate the capacity of bioLUNA sensor in eliminating background, either the fluorescent or bioluminescent signal of cpHNLuc$_4$-MB conjugate was measured in PBS buffer and blood. As shown in the added Figure S7, while the fluorescent signal of the sensor is distinct from the background in the PBS buffer (Figure S7A), the sensor's fluorescent signal is not very different from the background's fluorescent signal (Figure S7B), due to the autofluorescence of the blood sample. In contrast, the BRET signal of the sensor in the same blood sample (Figure S7D) is almost the same as the BRET signal in the buffer (Figure S7C). These results demonstrated that the bioLUNA can minimize background and have the potential for assay in complex environments.

In addition to the protein and DNA conjugation, the spectral overlap between the emission of energy donors and the absorption of the acceptor can also determine the efficiency of energy transfer. To achieve the best energy transfer efficiency, we evaluated the spectra of fluorophores that are commonly used to modify oligonucleotides (Figure S8), including fluorescein (FAM), cyanine 3 (Cy3), 5-carboxytetramethylrhodamine (TAMRA), and cyanine 5 (Cy5). The cpHNLuc$_4$ was labeled with the capture DNA strands L21, followed by the hybridization of complementary strands with one of the fluorophores. Based on the normalized BRET spectra of the fluorophores we tested (Figure 2D), the Cy3- and TAMRA-labeled DNA strands exhibited a relatively higher emission intensity, with a BRET ratio of nearly 4-fold (Figure 2D), and superior signal-to-background ratios of

51 and 59-fold, respectively (Figure S9). Therefore, Cy3 and TAMRA were the optimal energy receptors for the BRET-based bioLUNA sensors. Moreover, since the absolute bioluminescence intensity of NLuc is determined by the protein concentration and the consumption of substrate, the signals from such a reaction are often not consistent and thus can hinder quantitative analyses. This issue can be addressed by the ratiometric nature of the BRET sensor. As shown in Figure S10, the emission ratios do not shift in the presence of different concentrations of the sensor, suggesting the stability of this ratiometric BRET signal. These results demonstrated that the cpHNLuc$_4$ and Cy3 pair was a promising candidate for the construction of BRET bioLUNA sensors.

Construction of a BRET DNAzyme sensor

To construct a BRET DNAzyme sensor using the cpHNLuc$_4$ variant, we chose Zn^{2+}-specific 8–17 DNAzyme as a proof of concept, because it is the most well-studied and broadly used DNAzyme for cellular and *in vivo* applications,[21] and Zn^{2+} plays important roles in biological systems.[22] As shown in Figure 3A, the DNAzyme labeled with chloroalkane can be conjugated to cpHNLuc$_4$, followed by hybridization with a Cy3-modified substrate strand to form a BRET DNAzyme (bioLUNA-Dz) sensor. The high BRET signal should be observed between the protein and Cy3 with a supply of furimazine. In the presence of Zn^{2+}, the substrate strand would be cleaved by the DNAzyme and the Cy3-contained fragment would be released from the sensor due to the change in melting temperature. This release increased the distance between the protein and Cy3, which can cause an increased bioluminescence signal of cpHNLuc$_4$ and a decreased emission from Cy3. To investigate the activity of the sensor, SDS-PAGE was used to visualize the cleavage of the substrate strands. As shown in Figure S11, with the addition of Zn^{2+}, most of the substrate strand was cleaved. In contrast, the substrate strand remained intact in the absence of Zn^{2+}. This difference demonstrated the Zn^{2+}-dependent activity of bioLUNA-Dz.

Next, we investigate the quantitative relationship between the BRET signal and Zn^{2+} concentrations. After the bioLUNA-Dz sensor was incubated with different concentrations of Zn^{2+}, the emission spectra were recorded by fluorometer without turning on the excitation laser. As shown in Figure 3B, the sensor exhibited a higher BRET peak of Cy3 at 565 nm than the bioluminescence at 450 nm without Zn^{2+}, indicating the efficient BRET between the protein and Cy3. The Cy3 signal kept decreasing with increasing Zn^{2+} concentrations, while the bioluminescence of NLuc recovered. The metal ion titration curve showed that the BRET ratio (450 nm / 656 nm) increased from 0.27 to reach a plateau of 1.55 after the concentration of Zn^{2+} reached 40 μM (Figure 3C). A linear relationship was observed with Zn^{2+} concentrations ranging from 0.6 to 4 μM (Figure 3D), and a limit of detection (LOD) of 0.20 μM Zn^{2+} was achieved (calculated based on 3σ/ slope). Moreover, the selectivity of the sensor towards the common metal ions in the biological system was also investigated. The results demonstrated that the bioLUNA-Dz exhibited a nearly 6-fold BRET signal change in the presence of Zn^{2+}, while only the background signal was observed after incubation with other metal ions (Figure 3E).

Applying the BRET DNAzyme sensor for imaging metal ion *in vivo*.

To demonstrate the capability of this bioLUNA-Dz in imaging metal ions *in vivo*, we performed a subcutaneous test in BALB/c mice. The mice were continuously anesthetized with 2% isoflurane on the operating stage of *in vivo* imaging system (IVIS). The right leg was pretreated with reaction buffer (50 mM Tris, 150 mM NaCl, pH 7.4) containing 50 μM Zn^{2+} and the left leg was injected with an equal volume of reaction buffer without Zn^{2+} as a control. A 25 μL reaction buffer containing 20 nM bioLUNA-Dz sensor and furimazine (1:25 dilution) was injected into each leg. The luminescence signal of $cpHNLuc_4$ and Cy3 was collected to calculate the BRET ratio (NLuc / Cy3). As displayed in Figure 4A, the emission of both NLuc and Cy3 can be observed on the legs. While both the emissions from NLuc and Cy3 were found to decrease, the ratio of NLuc to Cy3 has been demonstrated to remain the same (see Figure S10), indicating that such a ratiometric sensor can overcome background fluctuations. The quantification results in Figure 4B showed a comparable BRET ratio (NLuc / Cy3) on both legs after the initial injection and the ratio was observed to keep increasing on the right leg pretreated with Zn^{2+}, while the control group did not show appreciable change of the signal. After a reaction time of 20 min, the right leg of the mice showed a 1.8-fold increase in BRET ratio compared with the left leg, demonstrating the successful performance of the bioLUNA-Dz sensor *in vivo*.

After demonstrating the ability of bioLUNA-Dz in imaging metal ions *in vivo*, the sensor was further applied to detect Zn^{2+} in prostate cancer (PCa) in mice (Figure 4C). Males have a high concentration of mobile Zn^{2+} in their healthy prostate cells, but this level decreases dramatically in prostate cancer cells.[23] With the stimulation of D-glucose, the normal human epithelial prostate cells can secrete Zn^{2+} and subsequential increase the extracellular Zn^{2+} concentration, while the zinc-deficient prostate cancer cells fail to change the level of Zn^{2+} in their cellular microenvironment. If this difference in Zn^{2+} secretion can be identified by our bioLUNA-Dz sensor, the BRET signal changes could be used for the diagnosis of prostate cancer.[24] To demonstrate the diagnostic potential of our sensor, DU145-Luc, a human prostate cancer cell line that stably expresses firefly luciferase was xenografted into the ventral prostate of immunodeficient mice (NOD-SCID/Sja). The growth of the tumor could be visible by the bioluminescent signal of the luciferase after intraperitoneal (i.p.) injection of D-luciferin, the substrate of firefly luciferase (Figure S12). The mice were fasted for 12 hours prior to the anaesthetization by i.p. injection of chloral hydrate. An 8 mm incision was made on the hypogastrium to expose the prostate. Then, 25 μL of reaction buffer containing 50 nM of bioLUNA-Dz sensor and furimazine (4: 25 dilution) were orthotopically injected into the ventral prostate of the healthy prostate or the tumor site. The bioluminescent imaging was collected after a reaction time of 20 minutes. Subsequently, D-glucose was then injected to stimulate the secretion of Zn^{2+}, followed by the collection of BRET signal after another 20 minutes. Compared to the low BRET ratio (NLuc / Cy3) before the injection of glucose, a remarkable increase in the BRET ratio (2.68 times) was observed in the prostate after glucose stimulation, resulting from Zn^{2+} secretion by normal prostate cells. In contrast, the DU145 tumor exhibited a significantly lower BRET ratio either before or after glucose stimulation. These results are consistent with the Zn^{2+}-deficient environment of poorly differentiated adenocarcinoma (Figure 4D and 4E). Noticeably, the BRET signaling was similar in healthy prostate tissue and PCa tissue before

glucose stimulation, indicating that the Zn^{2+} deficiency was mainly inside of cancer cells but not in the tumor microenvironment. Finally, the mice were sacrificed and the prostates were taken out to further confirm the formation of prostate tumors (Figure S13). These results demonstrated that the bioLUNA-Dz sensor offered an effective and reliable tool for ratiometric metal ions imaging *in vivo*.

Conclusion

In conclusion, we have successfully developed an efficient strategy for designing bioluminescent nucleic acid (bioLUNA) sensors, which to our knowledge, is the first demonstration of a DNA sensor for bioluminescent imaging *in vivo*. This objective was achieved by rational protein engineering of a biorthogonal HaloTag-luciferase fusion, which allowed significant improvement of the catalytic efficiency for oligonucleotide labeling and BRET between the protein and the fluorophore on DNA sensors. As a proof of concept, a Zn^{2+}-dependent DNAzyme sensor was integrated into the protein. The sensor exhibited a low BRET ratio (D/A) initially, while a significantly increased BRET ratio (D/A) was observed in the presence of Zn^{2+}. The sensor imaged exogenous Zn^{2+} *in vivo*, as well as the endogenous Zn^{2+} efflux in normal epithelial prostate and prostate tumor, making it a powerful tool for monitoring metal ions in metabolic processes and providing pivotal information for metal ions involved in medicine. Since several DNAzymes have been reported to be selective for other metal ions, the demonstrated BRET sensor can be expanded to bioluminescent sensors for other metal ions by replacing the Zn^{2+} DNAzyme with other DNAzymes.[25] It is also possible to expand this bioluminescent sensor to use other nucleic acids, such as DNA/RNA aptamers.[26] Therefore, our work may stimulate other groups to apply the engineered cpHNLuc in constructing other bioluminescent nucleic acid sensors.

Supplementary Material

Refer to Web version on PubMed Central for supplementary material.

Acknowledgements

This work was supported by the National Natural Science Foundation of China (21890744) to X.B.Z. and (22104032) to M.Y.X, the National Key R&D Program of China (2019YFA0210100) to X.B.Z., the China Postdoctoral Science Foundation (2020M672470) to M.Y.X., the National Postdoctoral Program for Innovative Talents (BX2020118) to M.Y.X. and the US National Institute of Health (GM141931) to Y. L.

References

[1]. Carter KP, Young AM, Palmer AE, Chem. Rev. 2014, 114, 4564–4601. [PubMed: 24588137]

[2]. Barnham KJ, Bush AI, Chem. Soc. Rev. 2014, 43, 6727–6749. [PubMed: 25099276]

[3]. Pohl P, Trac-Trend. Anal. Chem. 2009, 28, 117–128.

[4]. Becker JS, Matusch A, Depboylu C, Dobrowolska J, Zoriy MV, Anal. Chem. 2007, 79, 6074–6080. [PubMed: 17622184]

[5]. Lemelle L, Simionovici A, Schoonjans T, Tucoulou R, Enrico E, Salome M, Hofmann A, Cavalazzi B, Trac-Trend. Anal. Chem. 2017, 91, 104–111.

[6]. a)Zeng L, Miller EW, Pralle A, Isacoff EY, Chang CJ, J. Am. Chem. Soc. 2006, 128, 10–11; [PubMed: 16390096] b)Chyan W, Zhang DY, Lippard SJ, Radford RJ, Proc. Natl. Acad.

Sci. USA 2014, 111, 143–148; [PubMed: 24335702] c)Zhou L, Zhang X, Wang Q, Lv Y, Mao G, Luo A, Wu Y, Wu Y, Zhang J, Tan W, J. Am. Chem. Soc. 2014, 136, 9838–9841; [PubMed: 24967610] d)Goldberg JM, Wang F, Sessler CD, Vogler NW, Zhang DY, Loucks WH, Tzounopoulos T, Lippard SJ, J. Am. Chem. Soc. 2018, 140, 2020–2023. [PubMed: 29384658]

[7]. Huang X, Meng J, Dong Y, Cheng Y, Zhu C, Polymer 2010, 51, 3064–3067.

[8]. a)Miyawaki A, Llopis J, Heim R, McCaffery JM, Adams JA, Ikurak M, Tsien RY, Nature 1997, 388, 882–887; [PubMed: 9278050] b)Qin Y, Dittmer PJ, Park JG, Jansen KB, Palmer AE, Proc. Natl. Acad. Sci. USA 2011, 108, 7351–7356. [PubMed: 21502528]

[9]. a)Lake RJ, Yang Z, Zhang J, Lu Y, Acc. Chem. Res. 2019, 52, 3275–3286; [PubMed: 31721559] b)Santoro SW, Joyce GF, Proc. Natl. Acad. Sci. USA 1997, 94, 4262–4266; [PubMed: 9113977] c)Breaker RR, Joyce GF, Chem. Biol. 2014, 21, 1059–1065; [PubMed: 25237854] d)Liu JW, Cao ZH, Lu Y, Chem. Rev. 2009, 109, 1948–1998. [PubMed: 19301873]

[10]. a)McGhee CE, Yang Z, Guo W, Wu Y, Lyu M, DeLong CJ, Hong S, Ma Y, McInnis MG, O'Shea KS, Lu Y, ACS Cent. Sci. 2021, 7, 1809–1820; [PubMed: 34841055] b)Torabi SF, Wu P, McGhee CE, Chen L, Hwang K, Zheng N, Cheng J, Lu Y, Proc. Natl. Acad. Sci. USA 2015, 112, 5903–5908; [PubMed: 25918425] c)Saran R, Liu JW, Anal. Chem. 2016, 88, 4014–4020; [PubMed: 26977895] d)Lin Y, Yang Z, Lake RJ, Zheng C, Lu Y, Angew. Chem. Int. Ed. 2019, 58, 17061–17067;e)Wang DY, Lai BHY, Feldman AR, Sen D, Nucleic Acids Res. 2002, 30, 1735–1742; [PubMed: 11937626] f)Huang PJJ, Liu JW, Nucleic Acids Res. 2015, 43, 6125–6133; [PubMed: 25990730] g)Huang PJJ, Liu JW, Anal. Chem. 2016, 88, 3341–3347; [PubMed: 26857405] h)Huang PJJ, Liu JW, Anal. Chem. 2014, 86, 5999–6005; [PubMed: 24851672] i)Liu JW, Brown AK, Meng XL, Cropek DM, Istok JD, Watson DB, Lu Y, Proc. Natl. Acad. Sci. USA 2007, 104, 2056–2061; [PubMed: 17284609] j)Wu Y, Torabi S-F, Lake RJ, Hong S, Yu Z, Wu P, Yang Z, Nelson K, Guo W, Pawel GT, Van Stappen J, Shao X, Mirica LM, Lu Y, Sci. adv. 2023, 9, eade7622; [PubMed: 37075105] k)Fan H, McGhee CE, Lake RJ, Yang Z, Guo Z, Zhang X-B, Lu Y, JACS Au 2023, 3, 1615–1622. [PubMed: 37388692]

[11]. a)Wang X, Kim G, Chu JL, Song T, Yang Z, Guo W, Shao X, Oelze ML, Li KC, Lu Y, J. Am. Chem. Soc. 2022, 144, 5812–5819; [PubMed: 35302361] b)Wu Y, Yang Z, Lu Y, Curr. Opin. Chem. Biol. 2020, 57, 95–104; [PubMed: 32652498] c)Yang ZL, Loh KY, Chu YT, Feng RP, Satyavolu NSR, Xiong MY, Huynh SMN, Hwang K, Li LL, Xing H, Zhang XB, Chelma YR, Gruebele M, Lu Y, J. Am. Chem. Soc. 2018, 140, 17656–17665. [PubMed: 30427666]

[12]. Choy G, O'Connor S, Diehn FE, Costouros N, Alexander HR, Choyke P, Libutti SK, Biotechniques 2003, 35, 1022–1030. [PubMed: 14628676]

[13]. a)Hall MP, Unch J, Binkowski BF, Valley MP, Butler BL, Wood MG, Otto P, Zimmerman K, Vidugiris G, Machleidt T, Robers MB, Benink HA, Eggers CT, Slater MR, Meisenheimer PL, Klaubert DH, Fan F, Encell LP, Wood KV, ACS Chem. Biol. 2012, 7, 1848–1857; [PubMed: 22894855] b)Xiong Y, Zhang Y, Li Z, Reza MS, Li X, Tian X, Ai HW, J. Am. Chem. Soc. 2022, 144, 14101–14111; [PubMed: 35913786] c)Yao Z, Zhang BS, Prescher JA, Curr. Opin. Chem. Biol. 2018, 45, 148–156. [PubMed: 29879594]

[14]. a)Yeh AH, Norn C, Kipnis Y, Tischer D, Pellock SJ, Evans D, Ma P, Lee GR, Zhang JZ, Anishchenko I, Coventry B, Cao L, Dauparas J, Halabiya S, DeWitt M, Carter L, Houk KN, Baker D, Nature 2023, 614, 774–780; [PubMed: 36813896] b)Chu J, Oh Y, Sens A, Ataie N, Dana H, Macklin JJ, Laviv T, Welf ES, Dean KM, Zhang F, Kim BB, Tang CT, Hu M, Baird MA, Davidson MW, Kay MA, Fiolka R, Yasuda R, Kim DS, Ng H-L, Lin MZ, Nat. Biotechnol. 2016, 34, 760–767. [PubMed: 27240196]

[15]. a)England CG, Ehlerding EB, Cai W, Bioconjug Chem 2016, 27, 1175–1187; [PubMed: 27045664] b)Tenda K, van Gerven B, Arts R, Hiruta Y, Merkx M, Citterio D, Angew. Chem. Int. Ed. 2018, 57, 15369–15373;c)Xue L, Yu Q, Griss R, Schena A, Johnsson K, Angew. Chem. Int. Ed. 2017, 56, 7112–7116;d)Zhang JZ, Yeh HW, Walls AC, Wicky BIM, Sprouse KR, VanBlargan LA, Treger R, Quijano-Rubio A, Pham MN, Kraft JC, Haydon IC, Yang W, DeWitt M, Bowen JE, Chow CM, Carter L, Ravichandran R, Wener MH, Stewart L, Veesler D, Diamond MS, Greninger AL, Koelle DM, Baker D, Nat. Biotechnol. 2022, 40, 1336–1340; [PubMed: 35484405] e)Griss R, Schena A, Reymond L, Patiny L, Werner D, Tinberg CE, Baker D, Johnsson K, Nat. Chem. Biol. 2014, 10, 598–603; [PubMed: 24907901] f)Su Y, Walker JR, Park Y, Smith TP, Liu LX, Hall MP, Labanieh L, Hurst R, Wang DC, Encell LP, Kim N, Zhang F, Kay MA, Casey KM, Majzner RG, Cochran JR, Mackall CL, Kirkland TA, Lin MZ, Nat.

Methods 2020, 17, 852–860; [PubMed: 32661427] g)Yu Q, Xue L, Hiblot J, Griss R, Fabritz S, Roux C, Binz P-A, Haas D, Okun JG, Johnsson K, Science 2018, 361, 1122–1126; [PubMed: 30213915] h)Iwano S, Sugiyama M, Hama H, Watakabe A, Hasegawa N, Kuchimaru T, Tanaka KZ, Takahashi M, Ishida Y, Hata J, Shimozono S, Namiki K, Fukano T, Kiyama M, Okano H, Kizaka-Kondoh S, McHugh TJ, Yamamori T, Hioki H, Maki S, Miyawaki A, Science 2018, 359, 935–939. [PubMed: 29472486]

[16]. a)Engelen W, van de Wiel KM, Meijer LHH, Saha B, Merkx M, Chem. Commun. 2017, 53, 2862–2865;b)van der Veer HJ, van Aalen EA, Michielsen CMS, Hanckmann ETL, Deckers J, van Borren M, Flipse J, Loonen AJM, Schoeber JPH, Merkx M, ACS Cent. Sci. 2023, 9, 657–667; [PubMed: 37122471] c)Zhang Y, Qian L, Wei W, Wang Y, Wang B, Lin P, Liu W, Xu L, Li X, Liu D, Cheng S, Li J, Ye Y, Li H, Zhang X, Dong Y, Zhao X, Liu C, Zhang HM, Ouyang Q, Lou C, ACS Synth. Biol. 2017, 6, 211–216. [PubMed: 27718551]

[17]. Hiblot J, Yu Q, Sabbadini MDB, Reymond L, Xue L, Schena A, Sallin O, Hill N, Griss R, Johnsson K, Angew. Chem. Int. Ed. 2017, 56, 14556–14560.

[18]. a)Erkelenz M, Kuo CH, Niemeyer CM, J. Am. Chem. Soc. 2011, 133, 16111–16118; [PubMed: 21919448] b)Chen RP, Blackstock D, Sun Q, Chen W, Nat. Chem. 2018, 10, 474–481. [PubMed: 29531373]

[19]. a)Kossmann KJ, Ziegler C, Angelin A, Meyer R, Skoupi M, Rabe KS, Niemeyer CM, Chembiochem 2016, 17, 1102–1106; [PubMed: 26972311] b)Wilhelm J, Kuhn S, Tarnawski M, Gotthard G, Tunnermann J, Tanzer T, Karpenko J, Mertes N, Xue L, Uhrig U, Reinstein J, Hiblot J, Johnsson K, Biochemistry 2021, 60, 2560–2575. [PubMed: 34339177]

[20]. a)Kompa J, Bruins J, Glogger M, Wilhelm J, Frei MS, Tarnawski M, D'Este E, Heilemann M, Hiblot J, Johnsson K, J. Am. Chem. Soc. 2023, 145, 3075–3083; [PubMed: 36716211] b)England CG, Luo H, Cai W, Bioconjug. Chem. 2015, 26, 975–986. [PubMed: 25974629]

[21]. a)Bonaccio M, Nucleic Acids Res. 2004, 32, 916–925; [PubMed: 14963261] b)Hwang K, Wu P, Kim T, Lei L, Tian S, Wang Y, Lu Y, Angew. Chem. Int. Ed. 2014, 53, 13798–13802.

[22]. Lee HJ, Korshavn KJ, Kochi A, Derrick JS, Lim MH, Chem. Soc. Rev. 2014, 43, 6672–6682. [PubMed: 24710074]

[23]. a)Ho E, Song Y, Curr. Opin. Clin. Nutr. 2009, 12, 640–645;b)Franklin RB, Milon B, Feng P, Costello LC, Front. Biosci. 2005, 10, 2230–2239. [PubMed: 15970489]

[24]. a)Clavijo Jordan MV, Lo ST, Chen S, Preihs C, Chirayil S, Zhang S, Kapur P, Li WH, De Leon-Rodriguez LM, Lubag AJ, Rofsky NM, Sherry AD, Proc. Natl. Acad. Sci. USA 2016, 113, E5464–E5471; [PubMed: 27562169] b)Yuan Y, Wei Z, Chu C, Zhang J, Song X, Walczak P, Bulte JWM, Angew. Chem. Int. Ed. 2019, 58, 15512–15517.

[25]. a)Xiong MY; Yang ZL; Lake RJ; Li JJ; Hong SN; Fan HH; Zhang XB; Lu Y, Angew. Chem. Int. Ed. 2020, 59, 1891–1896.b)Wu Y, Yang ZL, Lu Y, Curr. Opin. Chem. Biol. 2020, 57, 95–104. [PubMed: 32652498] c)Wang W, Satyavolu NSR, Wu Z, Zhang JR, Zhu JJ, Lu Y, Angew. Chem. Int. Ed. 2017, 56, 6798–6802.d)Wu Z, Fan H, Satyavolu NSR, Wang W, Lake R, Jiang JH, Lu Y, Angew. Chem. Int. Ed. 2017, 56, 8721–8725.e)Wu P, Hwang K, Lan T, Lu Y, J. Am. Chem. Soc. 2013, 135, 5254–5257. [PubMed: 23531046]

[26]. a)Zhao J, Gao J, Xue W, Di Z, Xing H, Lu Y, Li L, J. Am. Chem. Soc. 2018, 140, 578–581. [PubMed: 29281270] b)Wang D, Zhang J, Huang Z, Yang Y, Fu T, Yang Y, Lyu Y, Jiang J, Qiu L, Cao Z, Zhang XB, You Q, Lin Y, Zhao Z, Tan W, ACS Cent. Sci. 2023, 9, 72–83. [PubMed: 36712483] c)Meng HM, Liu H, Kuai H, Peng R, Mo L, Zhang XB, Chem. Soc. Rev. 2016, 45, 2583–2602. [PubMed: 26954935] d)Mou Q, Xue X, Ma Y, Banik M, Garcia V, Guo W, Wang J, Song T, Chen LQ, Lu Y, Sci. Adv. 2022, 8, eabo0902. [PubMed: 35767607]

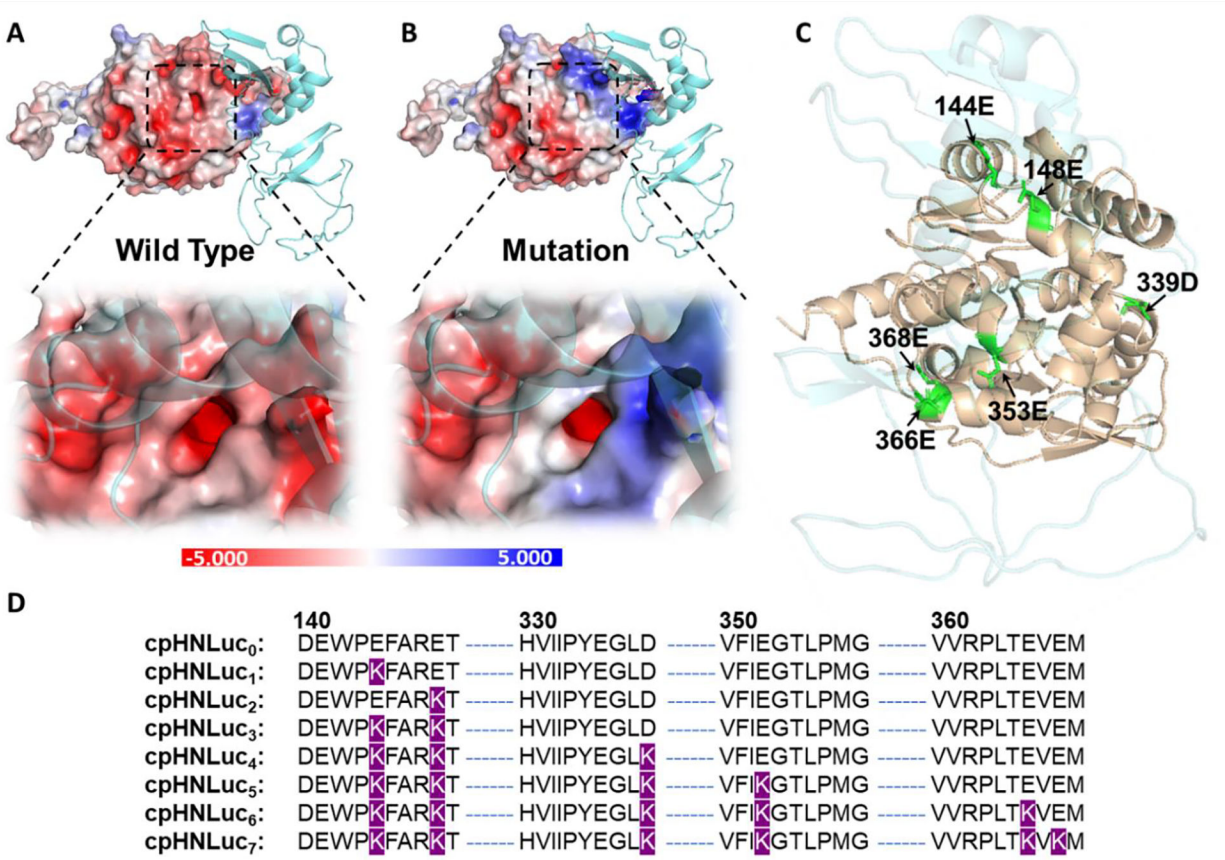

Figure 1.

Evolution of cpHNLuc for efficient labeling of DNA sensor. (A) Structure simulation of the cpHNLuc before ($cpHNLuc_0$) or (B) after ($cpHNLuc_4$) mutation. The carbon structure of cpNLuc was marked as cyan. The electrostatic potential of HaloTag protein and an enlarged view of the labeling site were displayed. The false color from red to blue indicates the electrostatic potential ranging from negative to positive. (C) The potential mutation sites (marked as green) on the carbon structure of cpHNLuc. (D) Peptide sequences of the variants containing mutation sites were highlighted in purple.

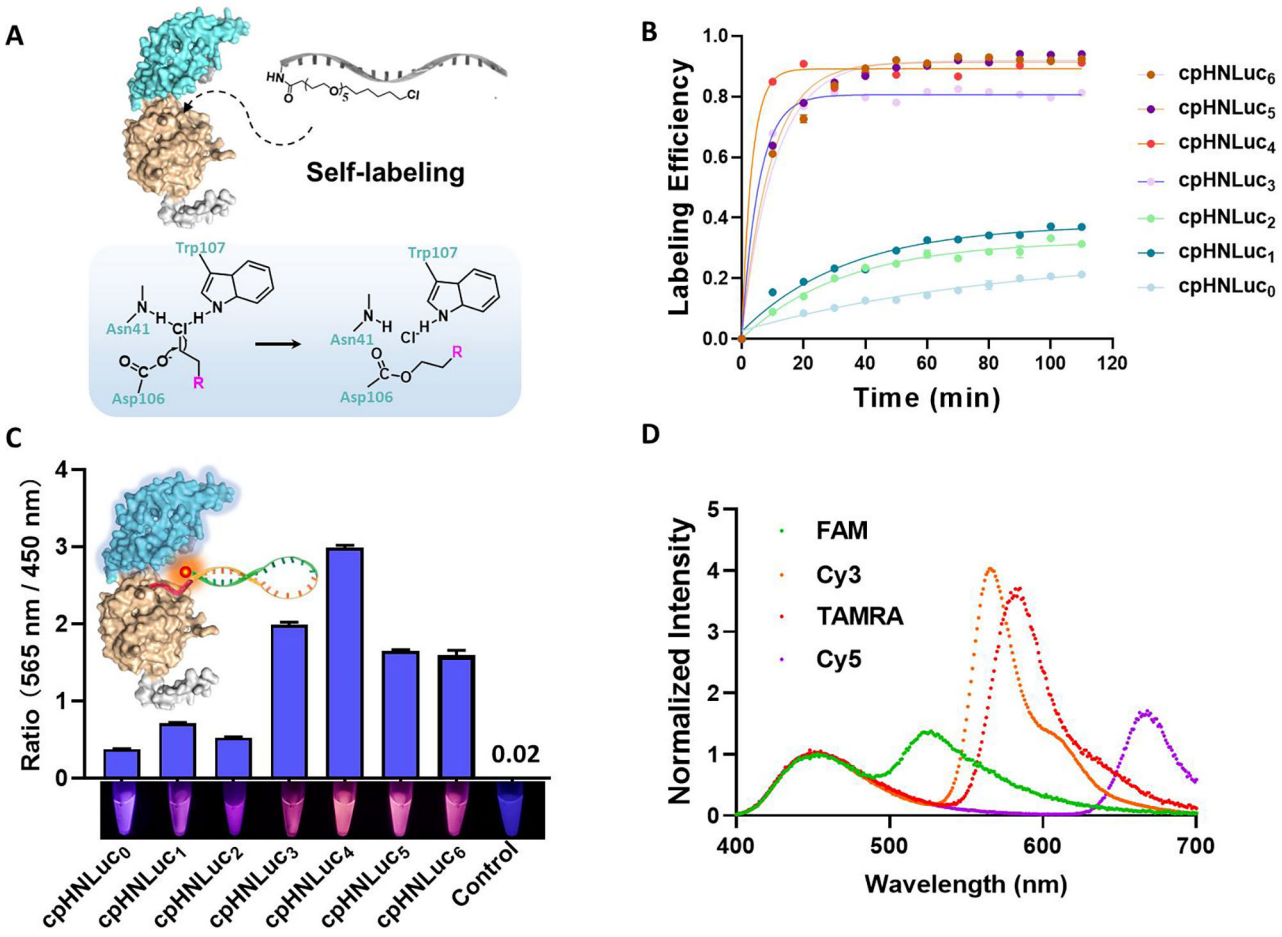

Figure 2.

(A) The self-labeling of chloroalkane molecule-modified oligonucleotides onto cpHNLuc variants. (B) Labeling kinetics of the variants toward oligonucleotides. (C) The BRET ratio (565 nm / 450 nm) and the photograph of the variants before (Control) and after modification with a fluorescent molecular beacon. (D) Emission spectra of $cpHNLuc_4$ labeled with a capture DNA strand and hybridized with indicated fluorophores labeled complementary strands. The intensity was normalized to $cpHNLuc_4$ maximum emission. Data are shown as mean ± SD (n=3).

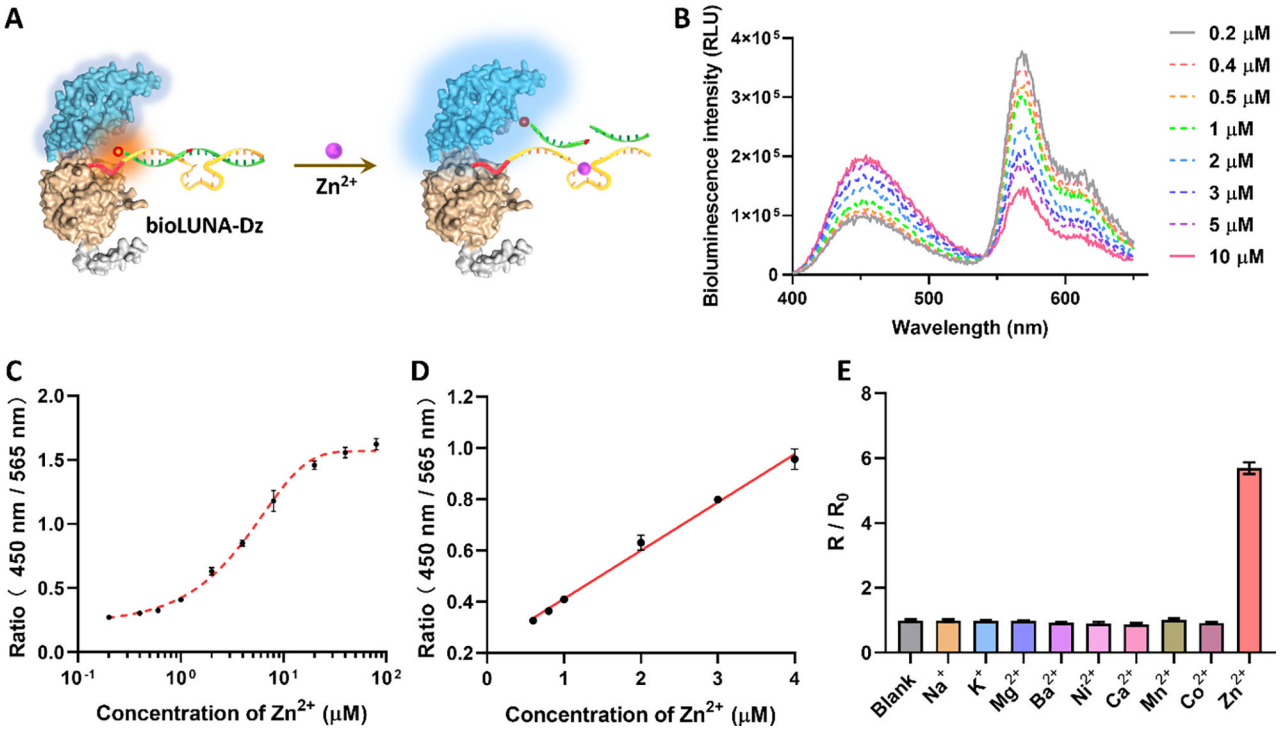

Figure 3.

(A) Design and working principle of the BRET-based DNAzyme sensor. (B) Emission spectra and (C) emission ratio of 20 nm sensor after reaction with various concentrations of Zn^{2+}. (D) The linear fitting curve of the sensor response to Zn^{2+} ranges from 0.6 to 4 μM. (E) The signal-to-background ratio of the sensor response to 100 μM of different metal ions. Data are shown as mean ± SD (n=3).

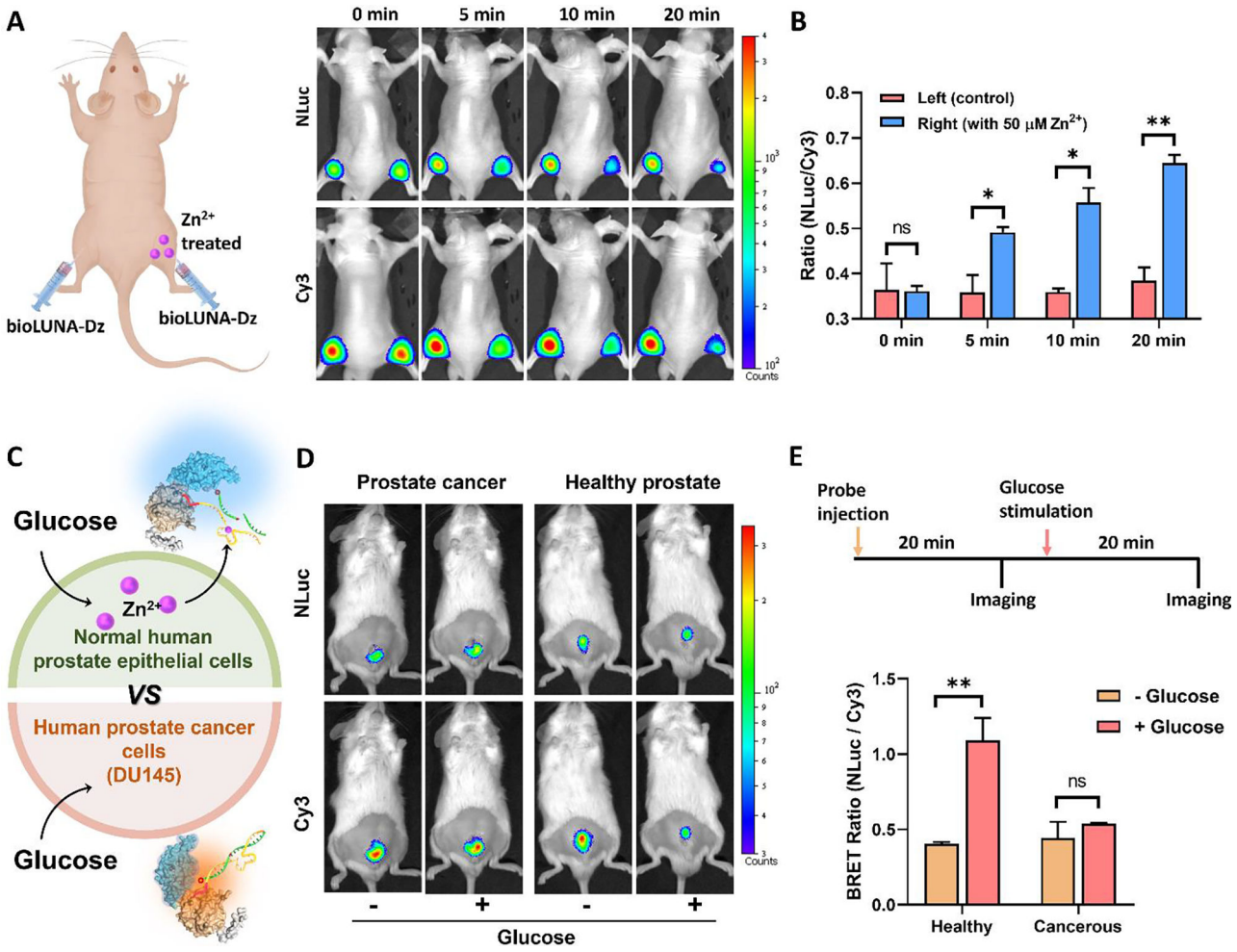

Figure 4.

The bioLUNA-Dz sensor for sensing *in vivo*. (A) Whole-body luminescence imaging of BALB/c mice after the injection of 20 nM sensor with or without 50 μM Zn^{2+} into the right or left leg, respectively. (B) Quantification of the emission ratio (NLuc / Cy3) on each leg at different reaction times. (C) Schematic of glucose-stimulated extracellular Zn^{2+} secretion with subsequent detection by bioLUNA-Dz sensor, which generates a signal in normal but not in cancerous prostate cells. (D) Luminescence imaging of DU145-bearing NOD-SCID/Sja mice and normal NOD-SCID/Sja mice before or after stimulation of glucose. Twenty-five microliters of 50 nM sensor were injected into the normal prostate or prostate tumor through an incision. The glucose-stimulated extracellular Zn^{2+} secretion was realized by i.p. injection of 100 μL of 20 % (w/v) D-glucose. (E) The scheme and statistical analysis of bioLUNA-Dz sensor and glucose injection. *p<0.1, **p<0.01. Data are shown as mean ± SD (n=3).

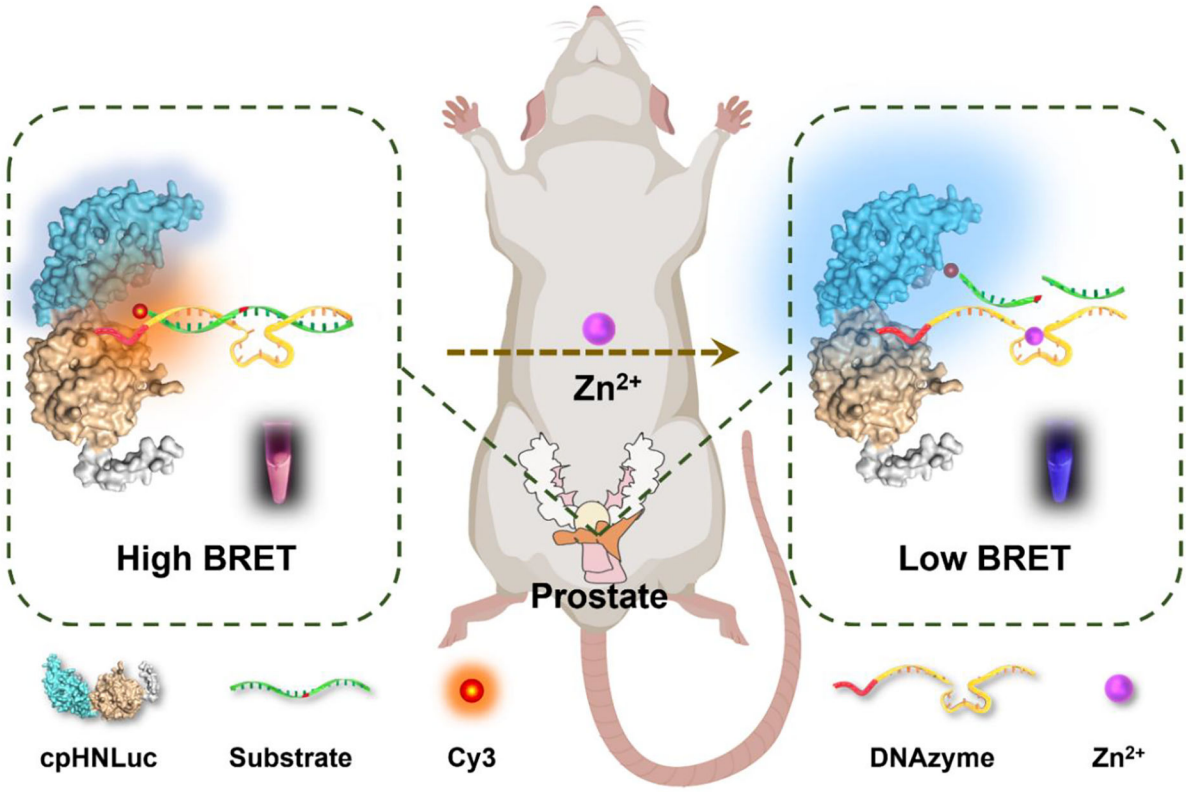

Scheme 1.

Structure of the semisynthetic bioluminescence DNAzyme sensor and its application in ratiometric detection of Zn^{2+} *in vivo*.